Environ Res Tec, Vol. 8, Issue. 4, pp. 963-976, December 2025

Environmental Research and Technology
https://dergipark.org.tr/en/pub/ert
DOI: https://doi.org/10.35208/ert.1551810

Research Article

River drinking water treatment using green-synthesized zinc oxide nanoparticles from Prosopis Glandulosa: Antibacterial efficiency and MB dye removal study

Muhammad Aqeel BHUTTO[1], Sheeraz Ahmed KHASKHELI[1], Farhatullah KANDHRO[2] Tanzeel Rehman CHARAN[1*], Siraj Hyder SOLANGI[3]

[1]University of Sindh, Institute of Biotechnology & Genetic Engineering, Jamshoro 76080, Pakistan
[2]Liaquat University of Medical and Health Sciences, College of Technology, Jamshoro 76090, Pakistan
[3]University of Sindh, Institute of Physics, Jamshoro 76080, Pakistan

ARTICLE INFO

Article history
Received: 18 September 2024
Revised: 17 January 2025
Accepted: 25 January 2025

Key words:
ZnO NPs, Prosopis glandulosa, methylene blue dye, antibacterial, river water treatment, adsorption kinetics and isotherm study

ABSTRACT

ZnO nanoparticles (NPs) were synthesized via a plant-mediated green synthesis method using aqueous extract from Prosopis glandulosa leaves. The synthesized NPs were characterized using UV-Vis spectroscopy, FTIR, XRD, and SEM, confirming their nanoscale morphology, polycrystalline structure, and an average size of 73.5 ± 6.7 nm. UV-Vis analysis revealed a maximum absorption peak at 340 nm, indicating a band gap energy of 3.44 eV, which is slightly higher than bulk ZnO due to quantum confinement effects. FTIR spectra exhibited key functional groups from the plant extract stabilizing the NPs. XRD analysis confirmed the hexagonal crystalline structure with peaks closely matching the JCPDS data card 01-079-0205. The ZnO NPs demonstrated remarkable efficiency in methylene blue dye removal, achieving a maximum removal rate of 95.24% at 100 mg/g dosage. Adsorption kinetics revealed pseudo-second-order behavior with an equilibrium capacity of 19.38 mg/g and a rate constant of 0.0289 g/mg/min, suggesting chemisorption as the dominant mechanism. Langmuir isotherm analysis yielded a maximum monolayer adsorption capacity of 88.5 mg/g, confirming favorable adsorption characteristics. Additionally, antibacterial activity evaluated through the disk diffusion method demonstrated significant inhibition of pathogenic bacteria. These findings highlight the potential of Prosopis glandulosa-synthesized ZnO NPs as an eco-friendly, cost-effective solution for water treatment, offering simultaneous antibacterial properties and efficient dye removal for the purification of Indus River drinking water.

Cite this article as: Bhutto MA, Khaskheli SA, Kandhro F, Charan TR, Solangi SH. River drinking water treatment using green-synthesized zinc oxide nanoparticles from Prosopis Glandulosa: Antibacterial efficiency and MB dye removal study. Environ Res Tec 2025;8(4) 963-976.

INTRODUCTION

The numerous uses of eco-friendly green synthesis of nanoparticles (NPs) in food, consumer goods, pharmaceuticals, and cosmetics have emerged in recent years. Such biogenic NPs have in the recent past been listed as being important functional entities involved in the fight against illnesses and the prevention of healthcare-associated infections [1]. Various metal oxide nanoparticles for instance; TiO_2, CuO, and ZnO have been green synthesized and used in multiple studies [2–4]. Among these metal oxide nanoparticles, ZnO NPs is the most interesting because they can be produced at low cost to obtain sufficient yield by the green synthesis method [5]. Thus, zinc oxide (ZnO), has many uses in elec-

***Corresponding author.**
*E-mail address: trcharan@scholars.usindh.edu.pk

tronics, optics, as well as in various healthcare applications [6]. The US Food and Drug Administration grouped ZnO under the safe metal oxide category [7].

Zinc oxide nanoparticles are of significant importance owing to their unique physical and chemical properties, such as a high exciton binding energy, large surface area-to-volume ratio, and wide band gap [8]. These characteristics of ZnO NPs are adaptable to a wide range of uses. For environmental remediation, ZnO NPs have presented significant photocatalytic activity, efficiently breaking down organic contaminants and sterilizing water from pathogenic microbes, thereby resolving water pollution problems [9, 10]. They are useful in biomedicine for targeted drug administration, cancer therapy, and antimicrobial therapies due to of their biocompatibility and potential to generate reactive oxygen species when exposed to UV radiation [11, 12]. Furthermore, because of ZnO NPs' great sensitivity and selectivity, they are used in sensors and biosensors, which allow for the accurate identification of chemical and biological species in environmental monitoring, food safety, and medical diagnostics [13].

The synthesis of nanoparticles by using an extract from medicinal plants is an innovative technique that has numerous uses such as in the medicinal field, agriculture, the food industry, as well as in water treatment [14–17]. The green synthesized nanoparticles are better than the nanoparticles synthesized using conventional chemical and physical methods because of the unique physicochemical finalities that plants inherited from the nanoparticles. Plants are endowed with great bio-chemicals, phytochemicals, and metabolites such as proteins, carbohydrates, fats, enzymes, coenzymes, and vitamins [18, 19]. Among all the chemical compounds of plants, the amount of flavonoids present in the plant extracts is very significant for the synthesis of ZnO NPs, as flavonoids have very potential for the synthesis of better nanoparticles [20]. Flavonoids are known for their strong antioxidant properties and ability to reduce metal ions, making them ideal for synthesizing nanoparticles through environmentally friendly processes. flavonoids contain functional groups necessary for nanoparticle synthesis, such as amine (-NH_2), carbonyl (-CO-), and hydroxyl (-OH). However the -OH group plays a very vital role in the synthesis of nanoparticles by reducing metal ions [21–23].

Numerous research studies have presented the synthesis of ZnO NPs with the help of extracts from different plants. However, to the best of our knowledge, there is scanty literature available in the scientific database on the green synthesis of ZnO NPs applying leaf extract of Prosopis glandulosa and their uses for the removal of dye colors, treatment of bacterial contamination, and removal of antibiotic substances from water. P.glandulosa has been reported as a medicinal plant in various studies due to its antiplasmodial, anticancer, antibacterial, antifungal, cardioprotective, antidiabetic, antimalarial, and antioxidant effects. Preliminary phytochemical screening of P.glandulosa revealed that the ethanolic extract contained alkaloids, sterols, glycosides, tannins, polyphenols, flavonoids, and terpenoids [24].

The various research papers also established that water-containing dyes, pathogens, and remains of antibacterial materials from any source such as textile, rubber, plastic, paper-making, printing, cosmetics, pharmaceutical industries, hospitals, and food industries is carcinogenic and toxic to living organisms. These are among the most dangerous pollutants in industrial wastewater, river water, and drinking water reservoirs [25, 26]. Also, these compounds tend to have an adverse impact on the aesthetic and water quality of the water in question. Hyderabad is one of the largest cities in Pakistan with a population reaching nearly two million people and is situated in the semi-arid area of Sindh province. The majority of the households in Hyderabad use treated water from the local water utility companies, however, the water supply is limited due to load shedding or power failure. Besides, the water is of poor quality because of poor treatment under such conditions and contamination by infiltration. Heavy metals, dye colors, and pathogenic microbes in the Indus River drinking water are serious issues. Therefore, water-containing dyes, microbes, and antibacterial drugs are among the most important environmental and public health threats. Recent studies have proved green synthesized ZnO NPs have antibacterial properties and strong effectiveness against various Gram +ve and Gram -ve pathogenic bacteria [8, 9, 12, 27, 28]. The ZnO NPs are also recognized as having great potential for removing dye compounds from contaminated water as an adsorbent [29].

The particular aim of the current study is to synthesize ZnO NPs from Prosopis glandulosa leaves extract using a green method; evaluate the antibacterial performance of the synthesized ZnO NPs against gram +ve and gram -ve bacteria; assess the effectiveness of ZnO NPs derived from Prosopis glandulosa in removing methylene blue (MB) dye from drinking water of the Indus River, commonly supplied to homes; and determine the applicability of linear adsorption isotherm and kinetic models.

MATERIALS AND METHODS

Preparation of 10 % Plant Extract

Fresh leaves of Prosopis glandulosa were thoroughly cleaned multiple times using deionized water to eliminate any dirt particles. Subsequently, the leaves were left open at room temperature for 4 hours. The leaves were ground into a fine powder through pestle and mortar. A total of 10 g of the fine powder was then mixed with 90 ml of double distal water and heated at 80 °C for 20 minutes. The powder mixture was filtered through Whatman no.1 filter paper to obtain an extract. The final volume of 100 ml was developed by adding further double distilled water. The extract solution was stored at 4 °C in a refrigerator until its further use in the synthesis of zinc oxide nanoparticles (ZnO NPs).

A 50 ml solution of zinc nitrate $Zn(NO_3)2.6H_2O$, having a concentration of 0.1 M, and 10 ml of Prosopis glandulosa aqueous extract were mixed through a magnetic stirrer at 28 °C for 3 hours and then centrifuged for 40 minutes at 8000 rpm [30]. The supernatant was decanted then the powder

precipitate was washed thrice with double-distilled water to ensure the purity of the nanoparticles. Subsequently, the nanoparticles were allowed to undergo natural curing, resulting in the formation of a solid material with a yellow color [31, 32].

The yellow solid material was dried for 12 hours in an incubator at 60 °C, forming a light brown powder. Further heating of this powder at 300 °C resulted in a final product that was a half-white powder. This obtained powder was stored in a dark bottle at 4 °C for subsequent experiments [33, 34]. The schematic diagram of the synthesis of zinc oxide nanoparticles is presented in Figure 1.

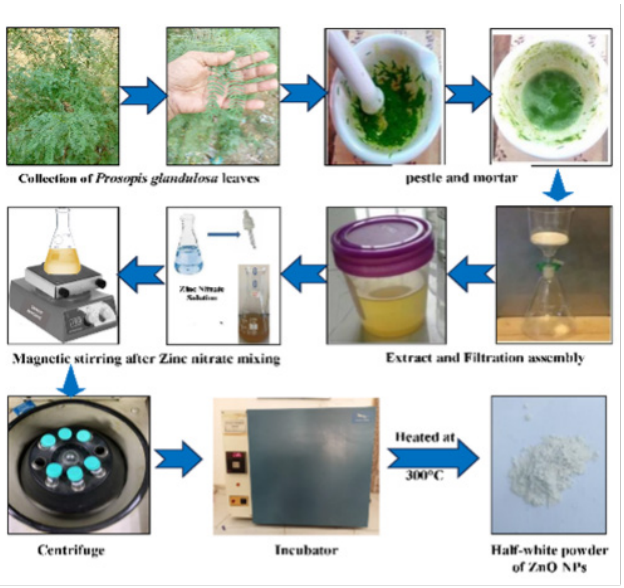

Figure 1. Schematic diagram for green synthesis of ZnO NPs from leaves of Prosopis glandulosa

Characterization of ZnO NPs of Prosopis glandulosa

Optical spectroscopy

The optical analysis of green synthesized ZnO NPs of P.glandulosa was performed by a UV-Vis spectrophotometer (wavelength 200 to 800 nm), by dissolving ZnO NPs in distilled water [35]. The the optical band gap (Eg) of ZnO nanoparticles was determined by Tauc plot by plotting $(ahv)^2$ versus hv [2].

$$(\propto hv)^2 = A(hv - Eg) \quad (1)$$

Where ∝ is the absorption coefficient, h is planck' constant, v is frequency of photon, A is constant and Eg is optical band gap of ZnO NPs.

FTIR analysis

The functional groups attached on the surface of ZnO NPs were analyzed by a Thermo-Scientific FTIR Spectrometer (Nicolet iS10. in the region of 4000–400 cm^{-1} at room temperature) [36]. Prior analysis, the samples were arranged in uniform dispersing ZnO NPs in a dry KBr matrix then clear pellets or disks were formed by compressing and crushing [37, 38].

X-Ray Diffraction (XRD) analysis

An X-ray diffractometer (XRD) was used to obtain diffraction patterns to evaluate the size of NPs, crystalline morphology, and surface structure. To obtain a diffraction pattern the radiation of Cu-K with a wavelength of λ=1.541 Å was applied [35]. The synthesized ZnO NPs samples in a thin film were placed in a glass slide for analysis. The X-ray diffraction pattern was recorded in 2θ value range of 4° to 80° at 0.002 minute and 1 second constant time. The X-ray diffractometer was optimized at a current of 30 mA and a voltage of 40 KV. The average grain size was analyzed by applying Scherrer's Equation No. (2), as given below.

$$D_p = \frac{0.9\,\lambda}{\beta\, Cos\,\theta} \quad (2)$$

Dp, λ, and θ represent the crystalline size, wavelength (1.5406 Å for Cu-K radiations), and angle of diffraction in radians respectively. β represents the FWHM (full width at half-maximum), and presents the light's wavelength.

Scanning Electron Microscopy (SEM) analysis

Morphological measurements of synthesized ZnO NPs were evaluated using images obtained from a scanning electron microscope (SEM), model JSM-6380L, in the range of 10-100 µm. Thin films for analysis were prepared by placing a single drop of ZnO NPs as 1 mg / 20 ml ratio in distilled water onto a carbon-coated grid. Then the carbon-coated grid was placed under the mercury lamp for 5 minutes to remove the solvent.

Methylene Blue Dye Removal Experiment

The efficiency of the MB dye removal of ZnO NPs of Prosopis glandulosa from home-supplied Indus River drinking water was evaluated by employing a UV spectrometer at the absorbance of 665 nm wavelength [39]. A stock solution of methylene blue dye (1000 mg /l) was prepared in double distilled water. Different concentrations (5 mg / l to 20 mg/l) were prepared from the stock solution of methylene blue dye.

Batch adsorption tests were performed to assess the dye removal efficiency at different dosages of adsorbent (10, 50, and 100 mg/l of solution), at various time intervals (30 to 90 minutes), and the effect of ZnO NPs on different methylene blue concentrations. The temperature was kept at 30 °C and the pH was kept at 6.8 using hydrochloric acid or 0.1 N sodium hydroxide. The adsorption temperature was regulated by utilizing a thermostatic water bath. For each adsorbent dosage, different glass tubes (100 ml River water) were prepared to contain different MB concentrations of 5 ppm, 10 ppm, 15 ppm, and 20 ppm of dye, and a 3 ml volume of the solution was used to measure the absorbance under a UV spectrophotometer used river water as a baseline. Using equations (3) and (4), the adsorption capacity qe (mg/g) and MB dye removal effectiveness R(%) were determined.

$$\text{Adsorption capacity } q_e = \frac{(Co-Ce)V}{M} \quad (3)$$

$$\text{The MB dye removal efficiency } R(\%) = \frac{(Co-Ce)}{Co}100 \quad (4)$$

Here, Co is the initial concentration of MB dye (mg/l), Ce is the liquid phase final concentration. M is the amount of adsorbent (ZnO NPs) and V is the total volume of solution.

Antibacterial Properties Analysis

The antibacterial properties of ZnO NPs of Prosopis glandulosa were determined by observing the zone of inhibition around ZnO NPs loaded disks in the disk diffusion method. A small portion of precultured microorganisms (gram -ve and gram +ve) previously procured from the Diagnostic and Research Laboratory, LUMHS Hyderabad, Pakistan, in Luria Bertani (LB) agar media, were transferred into 10 ml LB broth media [40]. Before the test procedures. The medium was incubated at 37 °C for 18 hours. Before inoculation, 0.5 McFarland standard was used to regulate the turbidity of the LB broth media at a concentration of 108 cells/ml. The bacteria were inoculated on agar medium plates using a sterilized swab. Also utilized were 6 mm disks. For 24 hours, all of the drug-loaded inoculation plates were incubated at 37 °C. The antimicrobial results of ZnO NPs were analyzed by observing and measuring the zones of inhibition (mm) including the size of the disk.

RESULTS AND DISCUSSIONS

Characterizations of ZnO NPs Green Dynthesized from Prosopis glandulosa

The ZnO NPs synthesis using Prosopis glandulosa extract showed a noticeable color change in the product. Primarily, the color transitioned from yellow to light brown after heat treatment at 60 °C in the incubator for 12 hours, and subsequently from brown to off-white by heating at 300 °C. After 3 hours, the final result was an off-white product. The production of ZnO NPs and the presence of phenolic and flavonoid chemicals in the Prosopis glandulosa extract are attributed to this color shift [21–23].

The literature has already documented that the temperature strongly influences the size of nanoparticles; the higher the temperature, the smaller the size of nanoparticles [41]. For moderate-sized nanoparticles, the reactant mixture was incubated at 60 °C. The color variations seen during the synthesis process lend support to the technique and are in line with previous findings on the synthesis of plant-mediated ZnO NPs, by other scientists [34, 37, 38].

Numerous techniques pertaining to the size, shape, chemistry, and qualitative and quantitative characterization of the produced ZnO NPs have been documented in the literature. X-ray diffraction, scanning electron microscopy, transmission electron microscopy, Fourier transform infrared spectrometry, ultraviolet-visible spectrometry, and energy-dispersive X-ray analysis are a few examples. Among these, UV spectroscopy is the method most often used to investigate the successful manufacture of zinc oxide nanoparticles. [25, 34, 35, 38, 42, 43].

The UV spectrum of the synthesized ZnO NPs using the extract of Prosopis glandulosa was obtained, and the results showed that its maximum absorption peak was around 339 nm in the present study (Figure 2). This result shows the synthesis of standard ZnO NPs because oxide materials or nanoscale materials themselves possess small wavelengths owing to their big band gap.

The comparison graph presented in Figure 2 clearly demonstrates the successful green synthesis of ZnO nanoparticles using P.Glandulosa. While the peak is not observed in the water extract of P.Glandulosa at the optimum wave length of ZnO NPs. The significant difference in absorbance between the ZnO NPs and the extract highlights the role of the plant extract in facilitating the formation of ZnO nanoparticles with enhanced optical properties [44, 45].

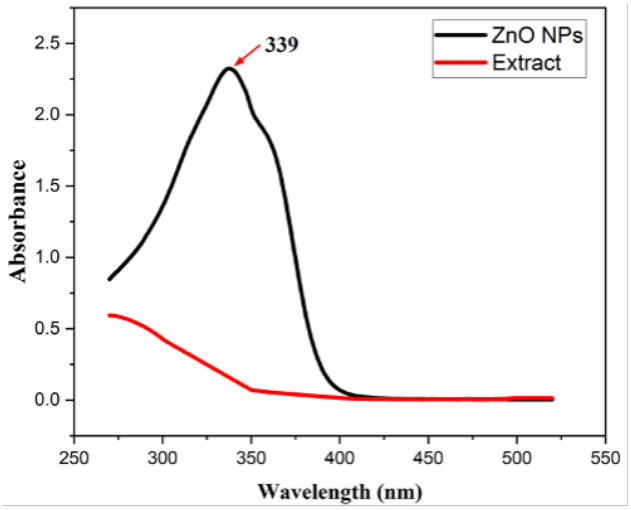

Figure 2. Uv-spectrometry analysis of ZnO NPs

Figure 3 shows the optical band gap (Eg) of ZnO nanoparticles is 3.44, slightly higher than the bulk ZnO (3.37 eV), which is attributed to the quantum confinement effect [46]. This increased band gap enhances the photocatalytic properties of ZnO nanoparticles, making them highly suitable for environmental applications such as drinking water purification and dye removal [47].

The higher band gap enables ZnO nanoparticles to effectively absorb UV light, generating reactive oxygen species (ROS) like hydroxyl radicals (OH) and superoxide anions (O_2) [48]. These ROS are capable of degrading organic pollutants, including harmful dyes and microorganisms, into less toxic or harmless byproducts [49]. The photocatalytic efficiency of ZnO nanoparticles under UV light ensures the removal of both chemical contaminants (e.g., industrial dyes) and biological impurities (e.g., bacteria) from water [50].

Furthermore, the stability, non-toxicity, and strong photocatalytic activity of ZnO nanoparticles make them an environmentally friendly and cost-effective choice for water treatment technologies. Their nanoscale size also enhances surface area, further improving their effectiveness in adsorbing and breaking down contaminants. The result highlights the potential of ZnO nanoparticles for practical applications in providing clean drinking water and addressing wastewater challenges in dye-laden industrial effluents.

The chemical nature and active functional groups in the

samples of ZnO NPs of Prosopis glandulosa plant extract were evaluated by FTIR spectroscopy. The detailed FTIR spectrum of ZnO NPs is presented in Figure 4, showing various absorption peaks at different wavelengths (cm^{-1}).

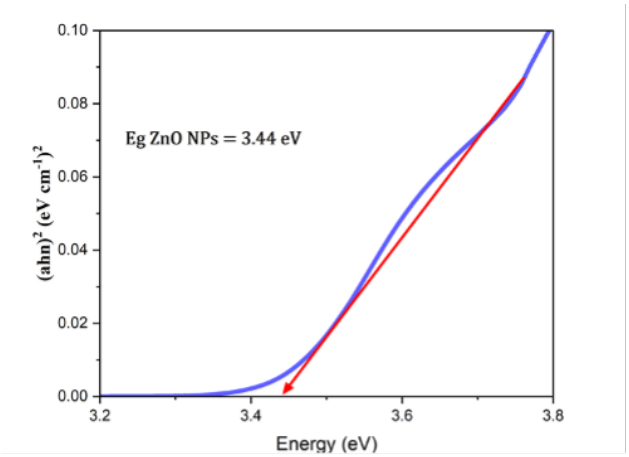

Figure 3. The optical band gap (Eg) of ZnO nanoparticles

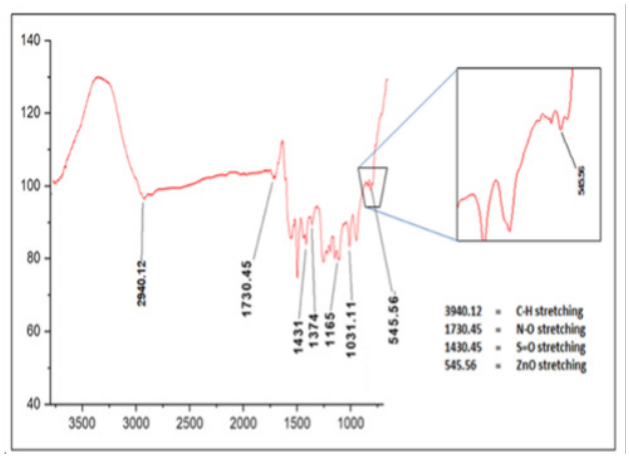

Figure 4. FTIR spectroscopy of green synthesized ZnO NPs from Prosopis glandulosa leaf extract

Briefly, a characteristic peak appeared at 2940 cm^{-1}, representing C-H stretching vibrations. The peak at 1730 cm^{-1} indicates C=O stretching, attributable to carbonyl groups from organic compounds in the plant extract. The short and sharp peaks around 1500-1600 cm^{-1} predominantly indicate N-H bending vibrations of amino acids or protein metabolites from the plant extract. Peaks at 1431 and 1374 cm^{-1} are due to C-H bonding, arising from various organic compounds or active metabolites of the plant. Peaks in the range of 1031-1165 cm^{-1} correspond to C-O stretching vibrations, which may be due to alcohol, ether, or carboxylic acid groups. The characteristic absorption band of ZnO is observed at 545 cm^{-1}, consistent with previous reports [51]. The presence of carbonyl and NH_2 groups from amino acids and protein residues contributes to the stabilization of nanoparticles. These compounds can bind to the metal and prevent agglomeration by generating a protective layer for the nanoparticles [52, 53].

The surface morphology of ZnO NPs was analyzed to determine the crystalline shape and size using an X-ray diffractometer (XRD). The XRD patterns of ZnO NPs synthesized from Prosopis glandulosa are presented in Figure 5, exhibiting peaks at 2θ values of 31.92°, 34.85°, 36.4°, 47.68°, 56.62°, 62.88°, 67.94°, and 69.09°. The present peaks indicate the crystalline ZnO NPs and are indexed to the (100), (002), (101), (102), (110), (103), (112), and (201) planes, respectively. The observed peaks match significantly with the JCPDS data card 01-079-0205, confirming the crystalline morphology and hexagonal structure of the ZnO NPs synthesized from Prosopis glandulosa. The average nanoparticle size of the synthesized ZnO, calculated using Scherrer's equation (Equation 2), was 14.98 ± 4.2 nm.

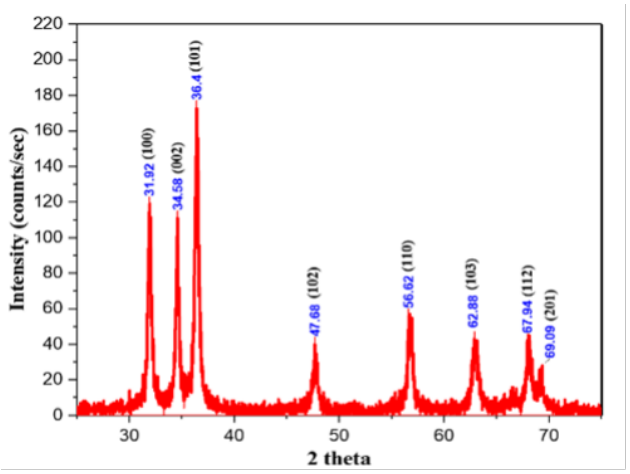

Figure 5. XRD spectra of ZnO NPs

The scanning electron microscopy (SEM) images of green synthesized ZnO NPs from the leaf extract of P.glandulosa are presented in Figure 6. The micrographs show that synthesized nanoparticles are predominantly spherical with a homogenous size distribution. The nanoparticles are clustered together and the surface of these aggregates appears rough. This agglomeration and clustering are attributed to the high surface energy of nanoparticles. The obtained SEM images also confirm that NPs are entirely pure, indicating that the Prosopis glandulosa plant has a strong capability to synthesize ZnO NPs. The nanoparticle diameter obtained from SEM is larger than the crystalline size calculated using the Scherrer equation from XRD data. This observation reveals the polycrystalline nature of nanoparticles which is an average size of 73.5 ± 6.7 nm. The overall morphology of the nanoparticles has a crucial role against pathogens, particularly spherical NPs that have a better ability to easily penetrate the cell walls of pathogens [54, 55]. Consequently, the green synthesized ZnO NPs from P.glandulosa show significant potential for treating clinical pathogenic bacteria.

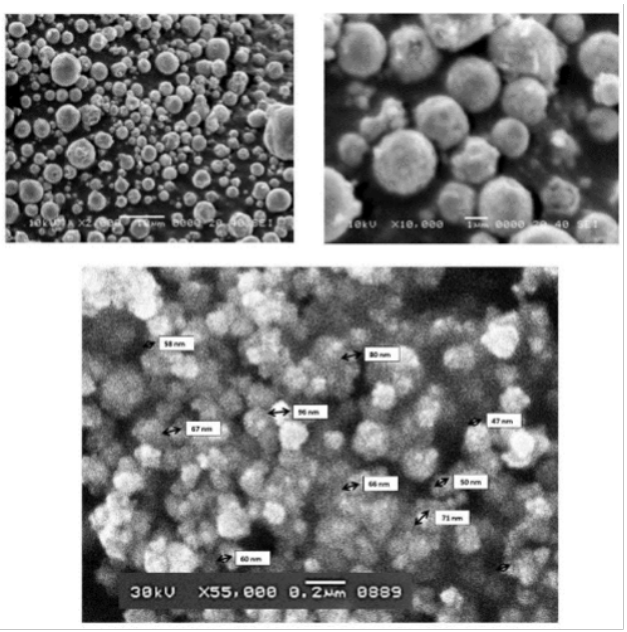

Figure 6. Scanning electron microscope images

Dye Removal Study

At a fixed pH of 6.8, the effect of contact duration on the adsorption capacity of various MB dye concentrations in river water incorporating ZnO NPs doses of 10 mg/g, 50 mg/g, and 100 mg/g was examined. The time intervals for the study were applied as 20, 40, 60, and 80 minutes. The details are presented in Table 1.

Table 1. Applied parameters for dye removal study

Sr. No.	Parameters	Value
1.	Contact time	20, 30, 40, 60, and 80 min.
2.	Initial Colour Concentration	5, 10,15 and 20 mg/L
3.	Adsorbent Dosage (ZnO Nps)	0.01, 0.05 and 0.1 g/g

Figures 7 (a), (b), and (c) show the removal rate (%) dramatically increased in all sample solutions with increased contact time and dosages. The maximum removal rate (R %) of dye at equilibrium was recorded in 5 ppm solutions: 93.936, 93.99, and 95.24 by applying adsorbent dosages of 10, 50, and 100 mg/g respectively. Initial fast adsorption was recorded in the early 20 minutes of dye contact with ZnO NPs, resulting in more than 80% removal in all samples of the study. This behavior could be noted since the surface of the nano adsorbent got saturated with MB dye ions, the adsorption and desorption processes. After 20 minutes, the further rate of removal becomes slow and decreases up to a concentration that is nearly equal to equilibrium; as the solution reaches the state of equilibrium, there is no alteration on the quantitative level. This is because, at the beginning of the reaction, all the active sites of the adsorbent may be available however the number will be saturated at some time.

The methylene blue dye removal is highly dependent on the potential of synthesized nanoparticles of ZnO and the effect of dosage. The adsorption capacity qe of ZnO NPs was assessed at dosages of 10, 50, and 100 mg/g in a 20 ppm MB dye solution at pH 6.8 after 1 hour, as presented in Figure 7(d). The observed data shows the adsorption capacities qe for ZnO NP dosages of 10, 50, and 100 mg/g are 183.84 ± 3.15, 35.93 ± 2.58, and 18.72 ± 3.35 mg/g, respectively. The corresponding MB dye removal was 92.14%, 39.4%, and 93.3%. These results present that as the dosage of ZnO nanoparticles increases, the adsorption capacity qe decreases significantly, while the removal efficiency (%) remains high and even improves slightly. This suggests that lower dosages yield higher adsorption capacity per unit weight, whereas higher dosages ensure more complete dye removal from the solution.

The effectiveness of various ZnO NP dosages on the removal of Methylene Blue (MB) dye was studied across different MB dye concentrations, as presented in Figure 8 (a) and (b). The removal efficiency increased with higher dosages of ZnO NPs. The maximum removal efficiencies were observed at an adsorbent dosage of 100 mg/g, achieving 95.2%, 94.96%, 94.6%, and 94.3% removal for 5 ppm, 10 ppm, 15 ppm, and 20 ppm MB dye concentrations, respectively. These results indicate that increasing the dosage of ZnO NPs increases the number of active sites available for adsorption. This enhancement allows more molecules of MB dye to interact with the surface of the adsorbent, thereby improving the dye removal percentage.

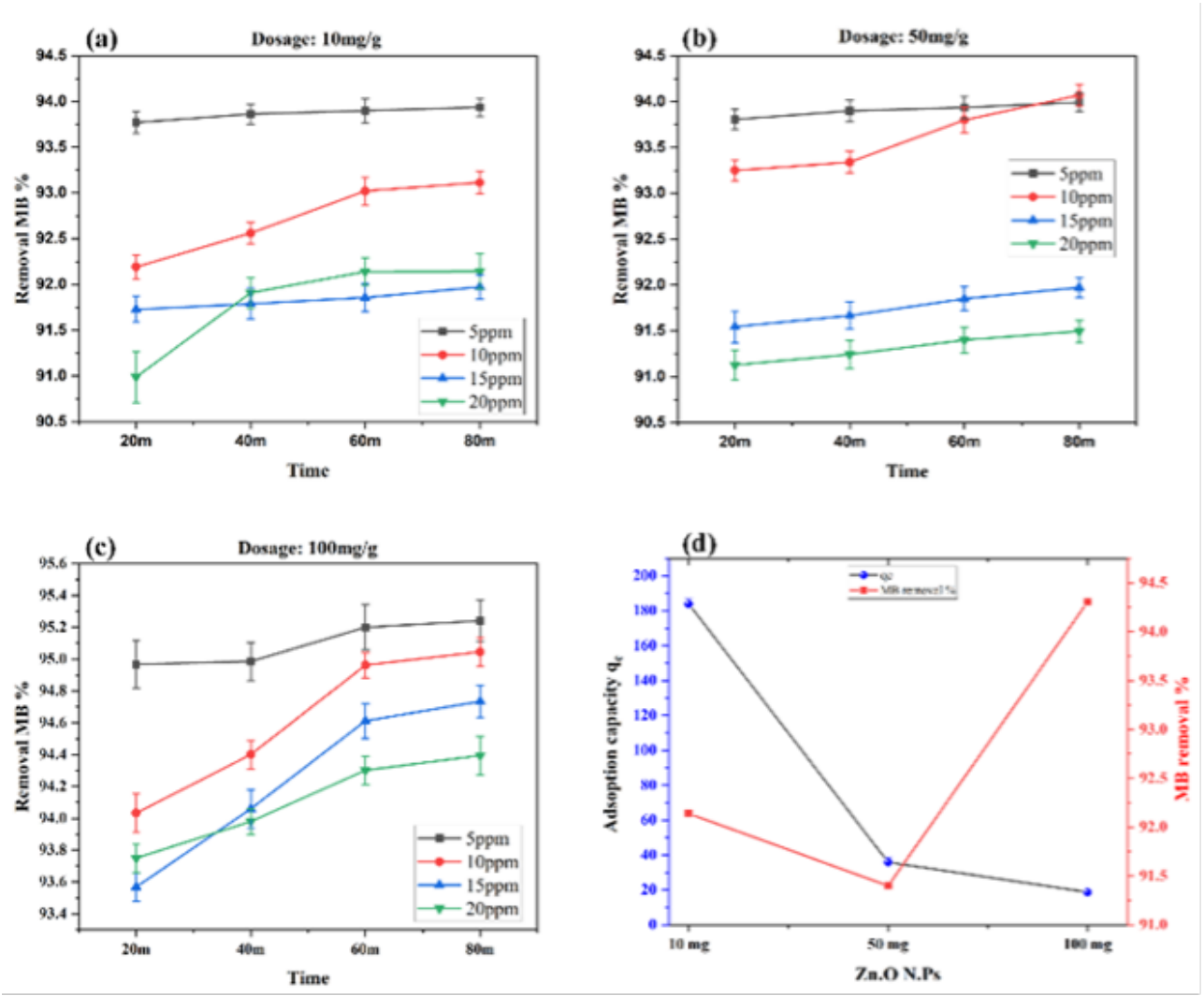

Figure 7. (a) MB dye removal at 10 mg/g of ZnO NPs (a) MB dye removal at 50 mg/g of ZnO NPs (c) MB dye removal at 100 mg/g of ZnO NPs. (d) the adsorption capacity of different ZnO NPs vs dye removal efficiency

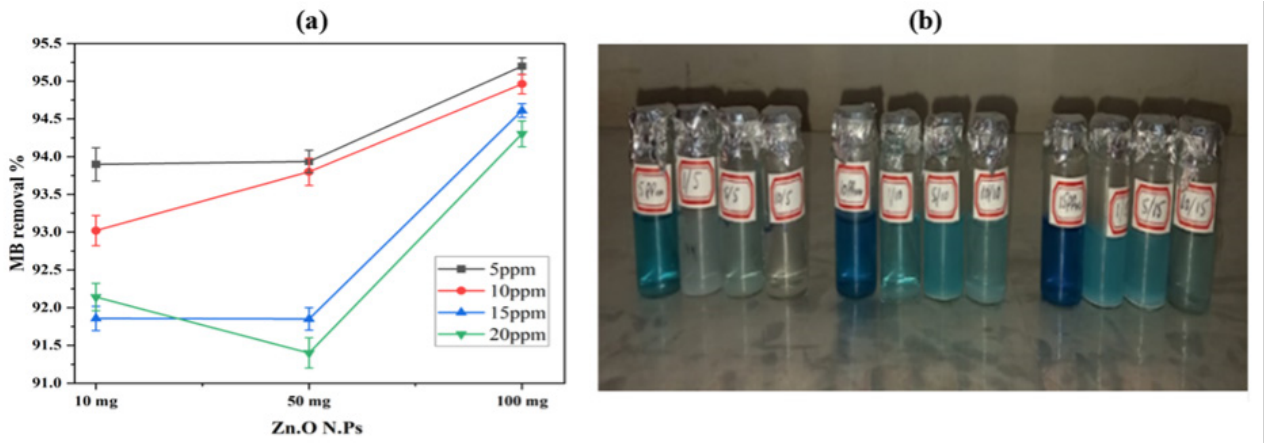

Figure 8. The effect of various ZnO NP dosages on the removal of Methylene Blue (MB) dye (a) presents a comparative graph and (b) samples of the study

Adsorption Kinetics and Isotherm Study

The dynamics of adsorption at a constant rate, the adsorption capacity, and the characteristics of the adsorbent and adsorbate are all determined by means of adsorption kinetics and isotherm research. The adsorption rate of any adsorbent is the critical factor for optimizing adsorbent dosage for the adsorption of the adsorbate. Consequently, a high adsorption ratio and excellent adsorption qualities are required of the adsorbent. Pseudo first order, pseudo second order, and intra-particle diffusion models are assessed to ascertain the kinetics of the adsorbent. A solution containing 20 ppm MB dye was adsorbed onto 100 mg/g of adsorbent and readings were noted at 10, 20, 40, 60, and 80 minutes. The pseudo first order kinetics was applied to evaluate the adsorption capacity of ZnO NPs for MB dye removal, as shown in Fig 8 (a), using the linearized form of the pseudo first order equation (5)

$$\log(q_e - q_t) = log\ q_e - \frac{k_1}{2.303} t \quad (5)$$

The calculated data from the applied pseudo first order demonstrates that the adsorption process follows pseudo first order kinetics, characterized by a rate constant k1 of 0.112 1/min and an equilibrium adsorption capacity qe of 8.89 mg/g. This indicates a relatively rapid adsorption process with substantial adsorption capacity. The linear regression model employed in establishing these parameters was satisfactory to the experimental data proving the suitability of the pseudo first order kinetic model in the current adsorption analysis.

The pseudo second order kinetic model is useful to obtain a much closer approximation to the adsorption process, for systems where the chemisorption is the dominant mechanism. It enhances acknowledgement of the kinetics, identification of the equilibrium capacity and facilitates the formulation of efficient adsorption systems. The pseudo second order kinetics was used, as shown in Figure 9 (b), using the linearized form of the pseudo second order equation (6).

$$\frac{t}{q_t} = \frac{1}{k_2 q_e^2} + \frac{t}{q_e} \quad (6)$$

The obtained data from the pseudo second order provides an equilibrium adsorption capacity qe of approximately 19.38 mg/g and a rate constant k2 of 0.0289 g/mg/min. This suggests that the adsorption process is probably regulated by chemisorption including valence forces through the sharing or exchange of electrons between the adsorbent and adsorbate. It also shows a good fit to the pseudo second order model.

The adsorption kinetics of ZnO NPs analysis by intra-particle diffusion model presented in Figure 9 (c) by applying equation (7)

$$q_t = k_{dif} \times t^{0.5} + C \quad (7)$$

The adsorption kinetics of ZnO NPs analysis by intra-particle diffusion model, presenting a relatively high slope Kdif 2.02586 mg/g.min-0.5 and intercept 4.32742 mg/g reveals a high diffusion rate within the particles and a notable boundary layer effect. The R2 value of 0.7621 shows that the model reasonably fits the experimental data, although other factors might also contribute to the adsorption process.

The adsorption mechanism can generally be divided into three stages: Surface Adsorption: This initial stage involves the rapid attachment of adsorbate molecules (MB dye) onto the external surface of ZnO nanoparticles. The rate of adsorption during this stage is governed primarily by external mass transfer processes and depends on the adsorbent's surface area and surface activity. Intra-Pore Diffusion: As the process continues, the adsorbate molecules diffuse into the interior pores of the adsorbent. This step is slower compared to surface adsorption and is influenced by the size and shape of the adsorbate, pore structure of the adsorbent, and diffusion properties of the system. In this study, the high slope Kdif highlights the significant contribution of intra-pore diffusion to the overall adsorption process. Equilibrium Stage: Finally, the adsorbate reaches equilibrium within the adsorbent's pores and on its surface, where the adsorption rate slows down, and no further significant adsorption occurs.

The intercept (C=4.32742 mg/g) indicates a substantial boundary layer effect, suggesting that surface adsorption plays a critical role in the early stages of the process. A higher C value typically corresponds to greater boundary layer resistance, reflecting the influence of surface interactions on the overall adsorption mechanism. Although the intra-particle diffusion model provides valuable insights, the R2 value (0.7621) indicates that the adsorption process is not solely controlled by intra-particle diffusion. This suggests the simultaneous contribution of surface adsorption and intra-pore diffusion to the adsorption mechanism, emphasizing the complex nature of the process. The results underscore the importance of considering both surface adsorption and intra-pore diffusion when analyzing the adsorption behavior of ZnO nanoparticles.

The kinetic adsorption parameters of ZnO NPs are presented in Table 2, which further supports the observed trends and highlights the suitability of ZnO nanoparticles for methylene blue dye removal.

In conclusion, the pseudo-second-order kinetic model, which accurately describes the adsorption mechanism, rate, and equilibrium capacity of ZnO nanoparticles for MB dye removal, is the most suitable kinetic model for the adsorption system for this study. The complementary contributions of surface adsorption and intra-pore diffusion further highlight the complex nature of the adsorption process.

The adsorption isotherms of adsorbent ZnO NPs and MB dye were evaluated hereby the linear formulation of the Langmuir model presented in equation (8).

$$\frac{c_e}{q_e} = \frac{1}{k_l \times q_m} + \frac{q_m}{c_e} \quad (8)$$

Fig 9 (a), and obtained data describe the adsorbent's high maximum adsorbent capacity (qm = 88.5 ml/g). Langmuir constant (kL=0.237) suggests a moderate affinity between

the adsorbent and adsorbate. The dimensionless separation factor (RL) ranges from 0.792 to 0.947 for the given concentrations, indicating favorable adsorption (since 0<RL<1). The adsorption study shows that the adsorbent has a high capacity and favorable adsorption characteristics for the adsorbate. These findings align well with the Langmuir adsorption isotherm model, which is indicative of a monolayer adsorption process with no significant migration or contact between the adsorbate molecules once adsorbed. The results suggest that the adsorbent is effective and can be utilized in practical applications where high adsorption capacity and favorable adsorption conditions are required.

The data of Freundlich isotherm is given in Table 3 and Figure 10 (b). Thus, the current change with respect to the adsorption process is directly proportional to pressure as explained by the model. The particularity of this model includes multilayer adsorption from heterogeneous systems, meeting the fact that the adsorption energies of several adsorption sites are different. The linear form of the isotherm is expressed logarithmically as follows equation (9):

$$log\, q_e = log\, K_F + \frac{1}{n} log C_e \quad (9)$$

where 1/n is the heterogeneous adsorption intensity constant and KF (1 g^{-1}) is the adsorption capacity constant. These values are derived from the intercept and slope of the logCe vs. $logqe$ plot.

In this study, the R2 value was 0.999, indicating a good fit of the data to the Freundlich model. The obtained n value of approximately 1.130 indicates favorable adsorption conditions, as n is greater than 1 and falls within the range of 1–10. This suggests that the adsorption process is indeed favorable. The high KF value of approximately 17.045 further indicates a significant capacity of the adsorbent to adsorb the adsorbate. Overall, the data demonstrates that the adsorption process is both favorable and effective, aligning well with the Freundlich isotherm model.

Antibacterial Properties Analysis of ZnO NPs

Using the disk diffusion method, the antibacterial qualities of ZnO NPs green synthesis from Prosopis glandulosa extract were examined. The findings are shown in Table 4 and Figure 11. By applying 25 and 50 µg/ml of ZnO NPs, the zone of inhibition surrounding the disks is measured to provide the antibacterial results. The antibacterial activity of ZnO NPs doses against S. aureus is 7.84 mm and 8.01 mm at 25 and 50 µg/ml, respectively. ZnO NPs exhibit antibacterial activity against E. coli of 8.83 mm and 9.1 mm at 25 and 50 µg/ml, respectively.

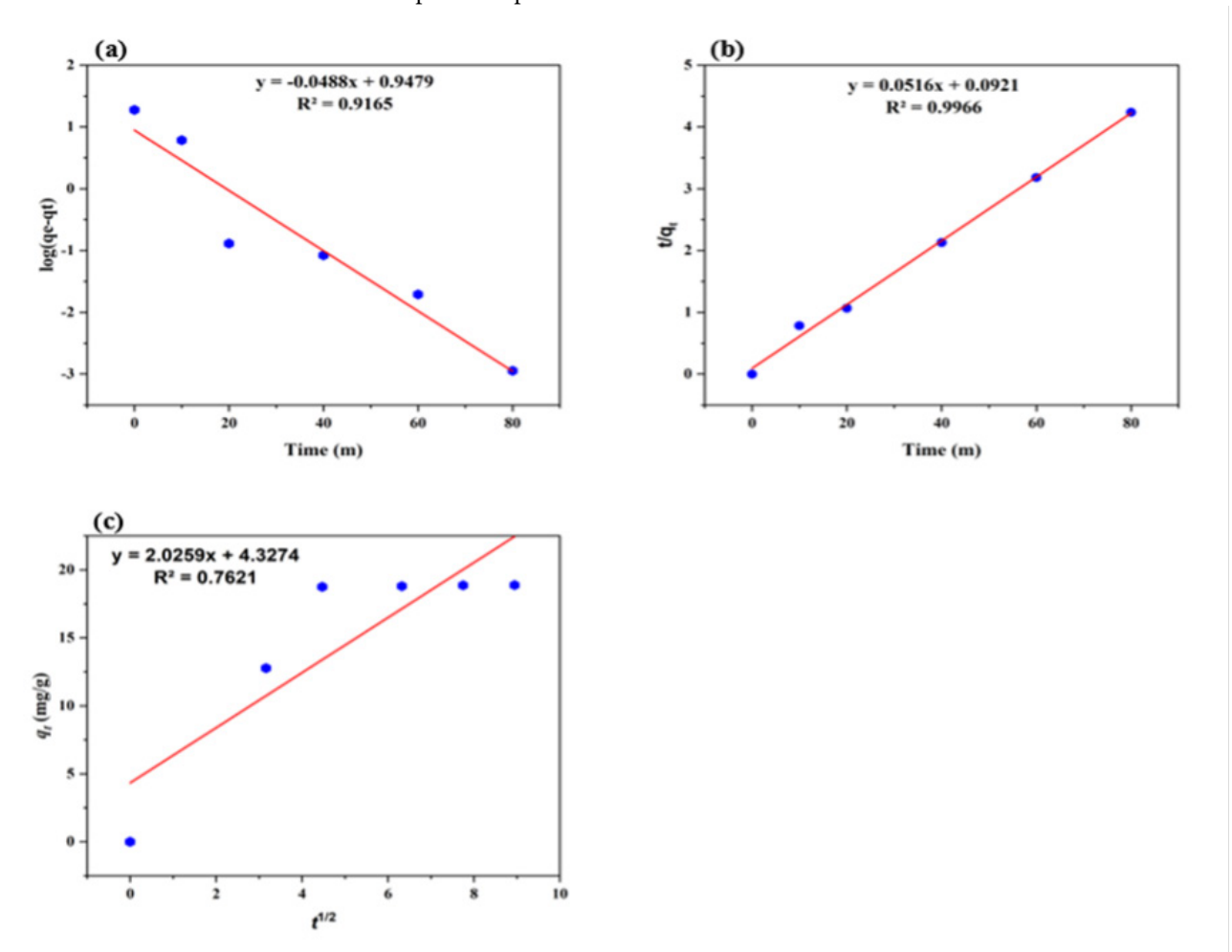

Figure 9. (a) Pseudo first order kinetics, (b) Pseudo second order kinetics, and (c) Intra particles diffusion

Table 2. Kinetic adsorption of ZnO NPs

Pseudo First Order		Pseudo Second Order		Intra-particles diffusion	
q_e	8.830799	q_e	19.37984	q_e	18.88
K_1	0.112386	K_2	0.029675	K_{dif}	2.02586
R_2	0.9165	R_2	0.9966	R_2	0.7621

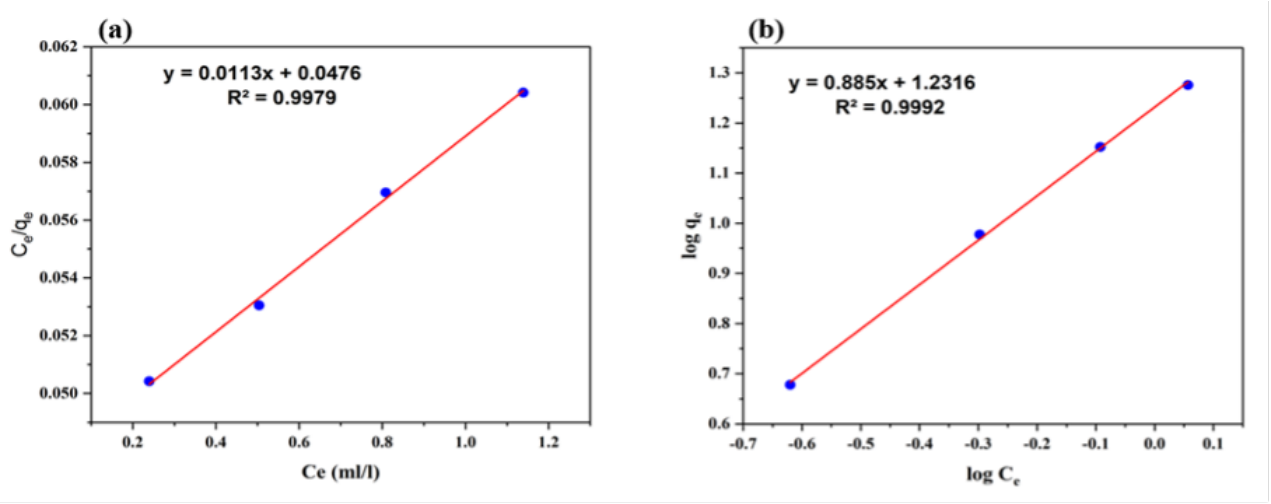

Figure 10. (a) Langmuir model (b) Freundlich model plots of Prosopis glandulosa ZnO NPs for adsorption of MB dye

Table 3. Isothermal study parameters of ZnO NPs

Langmuir isotherm model		Freundlich isotherm model	
k_L	0.237135	KF	17.04512
q_m	88.57396	N	1.129944
R_2	0.9979	R_2	0.9992

Table 4. Antibacterial activity of ZnO NPs

Genus	25 µg/ml ZnO NPs	50 µg/ml ZnO NPs
S.aureus	7.84±1.83	8.01±2.33
E.coli	8.83±0.88	9.1±2.42
S.aureus	7.84±1.83	8.01±2.33

According to the disk diffusion method, the current antibacterial investigation shows that zinc oxide nanoparticles (ZnO NPs), which were produced using a green synthesis approach using Prosopis glanddisulosa extract, have strong antibacterial activity against both Gram-ve and +ve bacteria. The results show that the antibacterial activity rises with increasing ZnO NPs concentrations. The greater susceptibility of E. Coli to ZnO NPs in contrast to S. aureus implies different levels of bacterial response. These results suggest that green-synthesized ZnO NPs may be useful in antibacterial therapies, while more investigation is needed.

CONCLUSIONS

This study perfectly explained the synthesis of zinc oxide nanoparticles (ZnO NPs) using a plant-mediated method through green synthesis using the aqueous extract of the leaves of the Prosopis glandulosa plant. The synthesized ZnO NPs were confirmed by UV-Vis spectroscopy, FTIR, XRD, and SEM which confirm the particle size, shape, and chemical composition of the synthesized ZnO NPs. The nanoparticles that were synthesized aspirin were crystalline in shape, spherical, and highly pure. The average size of the prepared nanoparticles was 14.98 ± 4.2 nm, which was calculated by using Scherrer's equation from the result of XRD analysis.

Furthermore, the capability of ZnO NPs in degrading/removing MB dye from Indus River drinking water solutions was evaluated. The actual observed adsorption studies found that the ZnO NPs have a high dye removal efficiency, with a maximum of 95.24% at a dosage of 100 mg/g. The adsorption kinetics followed by pseudo first order, pseudo second order model, and intra-particle diffusion model, indicate rapid adsorption, with chemisorption as the primary mechanism and the intra-particles model reasonably fits the experimental data. Adsorption isotherms models like Langmuir and Freundlich, present that the adsorbent

is effective for the removal of dye and the adsorption process is both favorable and effective, aligning well with both models.

Unlike earlier studies focusing on chemical synthesis methods, our plant-mediated synthesis using Prosopis glandulosa extract not only ensures an environmentally benign process but also yields ZnO nanoparticles with enhanced photocatalytic properties and stability, making them particularly suitable for water purification applications. The synthesized ZnO nanoparticles hold significant promise for future applications in sustainable water treatment technologies, particularly in countries where affordable and efficient solutions are critical. Their demonstrated ability to simultaneously remove dye pollutants and inhibit bacterial growth positions them as a dual-functional material for integrated water purification systems.

Our study provides novel insights into the adsorption and photocatalytic mechanisms of ZnO nanoparticles synthesized through green methods. These findings pave the way for future research on doping or functionalizing these nanoparticles to further enhance their efficacy for environmental applications. One of the key novelties of our research is the utilization of P.glandulosa for the synthesis of ZnO nanoparticles. To the best of our knowledge, no previous research has been conducted using ZnO NPs synthesized from P.glandulosa. This plant is wild, common, and easily available, especially in the end regions of the Indus River, making it a highly advantageous and sustainable resource for nanoparticle synthesis.

The above advantages open new windows of research in a particular direction which, in the future, will benefit the inhabitants of the specific area. The use of locally abundant P.glandulosa for nanoparticle synthesis could provide a cost-effective and eco-friendly solution, addressing both environmental and public health challenges associated with water pollution.

Overall, the green synthesis of ZnO NPs from Prosopis glandulosa plant leaf extract not only provides an eco-friendly and cost-effective approach but also results in nanoparticles with significant antibacterial properties and dye removal capabilities. These overall findings suggest that ZnO NPs synthesized from Prosopis glandulosa have promising applications in water treatment, particularly for the removal of dyes and bacterial contaminants from drinking water sources such as the Indus River. Further research and development could lead to the practical implementation of these nanoparticles in large-scale water purification systems, contributing to improved public health and environmental sustainability.

ACKNOWLEDGEMENT

The research conducted and the writing of this article was completed at the University of Sindh's Institute of Biotechnology and Genetic Engineering, located in Jamshoro, 76080, Pakistan. Additionally, all authors kindly recognize using the resources and services offered by the University of Sindh's Institute of Biotechnology and Genetic Engineering. We appreciate and express our gratitude to Ghulam Murtaza Khuhro and Dr. Muhammad Rafique for their assistance with antibacterial activity and moral support.

DATA AVAILABILITY STATEMENT

The authors confirm that the data that supports the findings of this study are available within the article. Raw data that support the finding of this study are available from the corresponding author, upon reasonable request.

CONFLICT OF INTEREST

The author declared no potential conflicts of interest with respect to the research, authorship, and/or publication of this article.

USE OF AI FOR WRITING ASSISTANCE

Not declared.

ETHICS

There are no ethical issues with the publication of this manuscript.

REFERENCES

1. T. R. Charan, M. A. Bhutto, M. A. Bhutto, A. A. Tunio, G. M. Khuhro, S. A. Khaskheli, and A. A. Mughal, "'Nanomaterials of curcumin-hyaluronic acid': their various methods of formulations, clinical and therapeutic applications, present gap, and future directions," Future Journal of Pharmaceutical Sciences, vol. 7, no. 1, p. 126, Dec. 2021, doi: 10.1186/s43094-021-00281-9.
2. G. T. Canbaz, "Green Synthesis of CuO Nanoparticles Using Tragopogon porrifolius and Their Antioxidant and Photocatalytic Applications," Cumhuriyet Science Journal, vol. 44, no. 4, pp. 671–677, Dec. 2023, doi: 10.17776/CSJ.1329389.
3. M. U. Gürbüz, M. Koca, G. Elmacı, and A. S. Ertürk, "In situ green synthesis of MnFe2O4@EP@Ag nanocomposites using green tea extract: An efficient magnetically recyclable catalyst for the reduction of hazardous organic dyes," Applied Organometallic Chemistry, vol. 35, no. 6, p. e6230, 2021, doi: https://doi.org/10.1002/aoc.6230.
4. M. U. Gürbüz, G. Elmacı, and A. S. Ertürk, "In situ deposition of silver nanoparticles on polydopamine-coated manganese ferrite nanoparticles: Synthesis, characterization, and application to the degradation of organic dye pollutants as an efficient magnetically recyclable nanocatalyst," Applied Organometallic Chemistry, vol. 35, no. 8, p. e6284,

2021, doi: https://doi.org/10.1002/aoc.6284.
5. S. Anjum, M. Hashim, S. A. Malik, M. Khan, J. M. Lorenzo, B. H. Abbasi, and C. Hano, "Recent Advances in Zinc Oxide Nanoparticles (ZnO NPs) for Cancer Diagnosis, Target Drug Delivery, and Treatment.," Cancers, vol. 13, no. 18, Sep. 2021, doi: 10.3390/cancers13184570.
6. Y. Zhang, T. R. Nayak, H. Hong, and W. Cai, "Biomedical Applications of Zinc Oxide Nanomaterials," Current molecular medicine, vol. 13, no. 10, p. 1633, Dec. 2013, doi: 10.2174/1566524013666131111130058.
7. G. Bisht and S. Rayamajhi, "ZnO Nanoparticles: A Promising Anticancer Agent.," Nanobiomedicine, vol. 3, p. 9, 2016, doi: 10.5772/63437.
8. H. Agarwal, S. Venkat Kumar, and S. Rajeshkumar, "A review on green synthesis of zinc oxide nanoparticles – An eco-friendly approach," Resource-Efficient Technologies, vol. 3, no. 4, pp. 406–413, Dec. 2017, doi: 10.1016/J.REFFIT.2017.03.002.
9. J. Gaur, S. Kumar, M. Pal, H. Kaur, K. M. Batoo, J. O. Momoh, and Supreet, "Current trends: Zinc oxide nanoparticles preparation via chemical and green method for the photocatalytic degradation of various organic dyes," Hybrid Advances, vol. 5, p. 100128, Apr. 2024, doi: 10.1016/J.HYBADV.2023.100128.
10. S. Yildiz, G. T. Canbaz, and H. Mihçiokur, "Photocatalytic degradation of oxytetracycline using ZnO catalyst," Environmental Progress & Sustainable Energy, vol. 43, no. 4, p. e14384, Jul. 2024, doi: 10.1002/EP.14384.
11. P. K. Mishra, H. Mishra, A. Ekielski, S. Talegaonkar, and B. Vaidya, "Zinc oxide nanoparticles: a promising nanomaterial for biomedical applications," Drug Discovery Today, vol. 22, no. 12, pp. 1825–1834, 2017, doi: https://doi.org/10.1016/j.drudis.2017.08.006.
12. J. Jiang, J. Pi, and J. Cai, "The Advancing of Zinc Oxide Nanoparticles for Biomedical Applications.," Bioinorganic chemistry and applications, vol. 2018, p. 1062562, 2018, doi: 10.1155/2018/1062562.
13. N. Tripathy and D.-H. Kim, "Metal oxide modified ZnO nanomaterials for biosensor applications," Nano Convergence, vol. 5, no. 1, p. 27, 2018, doi: 10.1186/s40580-018-0159-9.
14. C. Hano and B. H. Abbasi, "Plant-Based Green Synthesis of Nanoparticles: Production, Characterization and Applications.," Biomolecules, vol. 12, no. 1. Switzerland, Dec. 2021. doi: 10.3390/biom12010031.
15. N. S. Alharbi, N. S. Alsubhi, and A. I. Felimban, "Green synthesis of silver nanoparticles using medicinal plants: Characterization and application," Journal of Radiation Research and Applied Sciences, vol. 15, no. 3, pp. 109–124, 2022, doi: https://doi.org/10.1016/j.jrras.2022.06.012.
16. N. A. Othi, A. Hanan, M. Y. Solangi, M. S. AlSalhi, S. Devanesan, M. A. Shar, M. A. Bhutto, M. I. Abro, and U. Aftab, "Facile preparation of amino acid-assisted Fe3O4 nanoparticles for low-density lipoprotein cholesterol removal," Chemical Papers, vol. 77, no. 12, pp. 7749–7759, Dec. 2023, doi: 10.1007/S11696-023-03040-7/METRICS.
17. A. S. Ertürk, G. Elmaci, and M. U. Gürbüz, "Reductant free green synthesis of magnetically recyclable MnFe2O4@SiO2-Ag core-shell nanocatalyst for the direct reduction of organic dye pollutants," Turkish Journal of Chemistry, vol. 45, no. 6, pp. 1968–1979, Jan. 2021, doi: 10.3906/kim-2108-2.
18. A. A. Tunio, S. H. Naqvi, Q. U. N. Tunio, T. Rehman Charan, M. A. Bhutto, and M. H. Mughari, "Determination of Antioxidant, Antimicrobial Properties with Evaluation of Biochemicals and Phytochemicals Present in Oscillatoria limosa of District Jamshoro, Pakistan," Yuzuncu Yıl University Journal of Agricultural Sciences, vol. 32, no. 3, pp. 538–547, Sep. 2022, doi: 10.29133/YYUTBD.1112896.
19. A. A. Tunio, S. H. Naqvi, Q. U. N. Tunio, T. Rehman Charan, M. A. Bhutto, M. H. Mughari, M. Rafiq, A. A. Tunio, A. S. Qureshi, T. R. Charan, M. A. Bhutto, and Z. Lashari, "Determination of Phytochemicals, Antimicrobial, Antioxidant and Allelopathic Effects of Fagonia cretica L., collected from Jamshoro, Pakistan," Yuzuncu Yil University Journal of Agricultural Sciences, vol. 32, no. 4, pp. 785–794, 2022, doi: 10.29133/yyutbd.1112896.
20. T. R. Charan, M. A. Bhutto, M. A. Bhutto, A. A. Tunio, G. Murtaza, U. Aftab, F. Kandhro, and S. A. Khaskheli, "'Comparative analysis by total yield, antimicrobial and phytochemical evaluation of curcuminoid of district Kasur: With its potential use and characterization in electrospinning nanofibers,'" https://doi.org/10.1177/15280837221111457, vol. 52, p. 152808372211114, Oct. 2022, doi: 10.1177/15280837221111457.
21. V. V Makarov, A. J. Love, O. V Sinitsyna, S. S. Makarova, I. V Yaminsky, M. E. Taliansky, and N. O. Kalinina, "'Green' nanotechnologies: synthesis of metal nanoparticles using plants.," Acta naturae, vol. 6, no. 1, pp. 35–44, Jan. 2014.
22. M. A. Saleemi, B. Alallam, Y. K. Yong, and V. Lim, "Synthesis of Zinc Oxide Nanoparticles with Bioflavonoid Rutin: Characterisation, Antioxidant and Antimicrobial Activities and In Vivo Cytotoxic Effects on Artemia Nauplii.," Antioxidants (Basel, Switzerland), vol. 11, no. 10, Sep. 2022, doi: 10.3390/antiox11101853.
23. H. Jan, M. Shah, A. Andleeb, S. Faisal, A. Khattak, M. Rizwan, S. Drouet, C. Hano, and B. H. Abbasi, "Plant-Based Synthesis of Zinc Oxide Nanoparticles (ZnO-NPs) Using Aqueous Leaf Extract of Aquilegia pubiflora: Their Antiproliferative Activity against HepG2 Cells Inducing Reactive Oxygen Species and Other In Vitro Properties.," Oxidative medicine and cellular longevity, vol. 2021, p. 4786227, 2021, doi: 10.1155/2021/4786227.
24. J. Sharifi-Rad, F. Kobarfard, A. Ata, S. A. Ayatollahi,

N. Khosravi-Dehaghi, A. K. Jugran, M. Tomas, E. Capanoglu, K. R. Matthews, J. Popović-Djordjević, A. Kostić, S. Kamiloglu, F. Sharopov, M. I. Choudhary, and N. Martins, "Prosopis Plant Chemical Composition and Pharmacological Attributes: Targeting Clinical Studies from Preclinical Evidence.," Biomolecules, vol. 9, no. 12, Nov. 2019, doi: 10.3390/biom9120777.

25. L. M. Mahlaule-Glory and N. C. Hintsho-Mbita, "Green Derived Zinc Oxide (ZnO) for the Degradation of Dyes from Wastewater and Their Antimicrobial Activity: A Review," Catalysts 2022, Vol. 12, Page 833, vol. 12, no. 8, p. 833, Jul. 2022, doi: 10.3390/CATAL12080833.
26. H. Ben Slama, A. C. Bouket, Z. Pourhassan, F. N. Alenezi, A. Silini, H. Cherif-Silini, T. Oszako, L. Luptakova, P. Golińska, and L. Belbahri, "Diversity of synthetic dyes from textile industries, discharge impacts and treatment methods," Applied Sciences (Switzerland), vol. 11, no. 14, p. 6255, Jul. 2021, doi: 10.3390/app11146255.
27. K. Ali, S. Dwivedi, A. Azam, Q. Saquib, M. S. Al-Said, A. A. Alkhedhairy, and J. Musarrat, "Aloe vera extract functionalized zinc oxide nanoparticles as nanoantibiotics against multi-drug resistant clinical bacterial isolates," Journal of Colloid and Interface Science, vol. 472, pp. 145–156, Jun. 2016, doi: 10.1016/J.JCIS.2016.03.021.
28. J. Nogueira, M. António, S. M. Mikhalev, S. Fateixa, T. Trindade, and A. L. Daniel-da-Silva, "Porous Carrageenan-Derived Carbons for Efficient Ciprofloxacin Removal from Water," Nanomaterials, vol. 8, no. 12, 2018, doi: 10.3390/nano8121004.
29. F. Mohammadi, Z. Farahmandkia, M. R. Mehrasbi, M. H. Mahmoudian, F. S. Tabatabaei, R. Mostafaloo, N. Ghafouri, and M. Asadi-Ghalhari, "Ciprofloxacin antibiotic removal from aqueous solutions by ZnO nanoparticles coated on ACA: modeling and optimization.," Environmental monitoring and assessment, vol. 195, no. 12, p. 1443, Nov. 2023, doi: 10.1007/s10661-023-12041-8.
30. E. Ts, T. G, B. G, M. P, C. Sh, and J. N, "Synthesis and Characterization of ZnO Nanoparticles," Физик сэтгүүл, 2022, [Online]. Available: https://api.semanticscholar.org/CorpusID:7886439
31. H. Agarwal, S. Venkat Kumar, and S. Rajeshkumar, "A review on green synthesis of zinc oxide nanoparticles – An eco-friendly approach," Resource-Efficient Technologies, vol. 3, no. 4, pp. 406–413, 2017, doi: https://doi.org/10.1016/j.reffit.2017.03.002.
32. K. Bhardwaj and A. K. Singh, "Bio-waste and natural resource mediated eco-friendly synthesis of zinc oxide nanoparticles and their photocatalytic application against dyes contaminated water," Chemical Engineering Journal Advances, vol. 16, p. 100536, 2023, doi: https://doi.org/10.1016/j.ceja.2023.100536.
33. S. Sabir, M. Arshad, and S. K. Chaudhari, "Zinc oxide nanoparticles for revolutionizing agriculture: synthesis and applications.," TheScientificWorldJournal, vol. 2014, p. 925494, 2014, doi: 10.1155/2014/925494.
34. F. Rahman, M. A. Majed Patwary, M. A. Bakar Siddique, M. S. Bashar, M. A. Haque, B. Akter, R. Rashid, M. A. Haque, and A. K. M. Royhan Uddin, "Green synthesis of zinc oxide nanoparticles using Cocos nucifera leaf extract: characterization, antimicrobial, antioxidant and photocatalytic activity," Royal Society open science, vol. 9, no. 11, Nov. 2022, doi: 10.1098/RSOS.220858.
35. A. S. Abdelbaky, T. A. Abd El-Mageed, A. O. Babalghith, S. Selim, and A. M. H. A. Mohamed, "Green Synthesis and Characterization of ZnO Nanoparticles Using Pelargonium odoratissimum (L.) Aqueous Leaf Extract and Their Antioxidant, Antibacterial and Anti-inflammatory Activities.," Antioxidants (Basel, Switzerland), vol. 11, no. 8, Jul. 2022, doi: 10.3390/antiox11081444.
36. M. A. Bhutto, M. A. Bhutto, G. S. Mangrio, T. R. Charan, and A. A. Tunio, "Study on the Viability and Sustainable Release of Rice Rhizobacteria (Paenibacillus IBGE-MAB1) İmmobilized in Nanofibers for Enhanced Rice Seed Coating and Germination," BioNanoScience, 2024, doi: 10.1007/s12668-024-01460-7.
37. M. Naseer, U. Aslam, B. Khalid, and B. Chen, "Green route to synthesize Zinc Oxide Nanoparticles using leaf extracts of Cassia fistula and Melia azadarach and their antibacterial potential," Scientific Reports, vol. 10, no. 1, pp. 1–10, Jun. 2020, doi: 10.1038/s41598-020-65949-3.
38. Sachin, Jaishree, N. Singh, R. Singh, K. Shah, and B. K. Pramanik, "Green synthesis of zinc oxide nanoparticles using lychee peel and its application in anti-bacterial properties and CR dye removal from wastewater," Chemosphere, vol. 327, p. 138497, 2023, doi: https://doi.org/10.1016/j.chemosphere.2023.138497.
39. S. Bagheri, F. Moghadam, H. Mohammadi, and S. Rigi, "The Removal of Methylene Blue from Aqueous Solutions Using Zinc Oxide Nanoparticles With Hydrogen Peroxide," Avicenna J Environ Health Eng, vol. 10, no. 1, pp. 32–37, 2023, doi: 10.34172/ajehe.2023.5259.
40. T. R. Rehman, M. A. M. A. Bhutto, M. A. M. A. Bhutto, A. A. Tunio, B. A. Baig, N. A. Tunio, A. A. Bhutto, G. S. Mangrio, T. R. Charan, and A. A. Tunio, "Isolation and characterization of curcumin by antisolvent and cooling crystallization method for a potential antimicrobial nanofibrous membrane," Nanomedicine Research Journal, vol. 8, no. 3, pp. 246–258, 2023, doi: 10.22034/nmrj.2023.03.003.
41. H. Hassan Basri, R. A. Talib, R. Sukor, S. H. Othman, and H. Ariffin, "Effect of Synthesis Temperature on the Size of ZnO Nanoparticles Derived from Pineapple Peel Extract and Antibacterial Activity of ZnO-Starch Nanocomposite Films.," Nanomaterials

(Basel, Switzerland), vol. 10, no. 6, May 2020, doi: 10.3390/nano10061061.

42. S. MalligArjuna Rao, S. Kotteeswaran, and A. M. Visagamani, "Green synthesis of zinc oxide nanoparticles from camellia sinensis: Organic dye degradation and antibacterial activity," Inorganic Chemistry Communications, vol. 134, p. 108956, 2021, doi: https://doi.org/10.1016/j.inoche.2021.108956.
43. S. T. Karam and A. F. Abdulrahman, "Green Synthesis and Characterization of ZnO Nanoparticles by Using Thyme Plant Leaf Extract," Photonics 2022, Vol. 9, Page 594, vol. 9, no. 8, p. 594, Aug. 2022, doi: 10.3390/PHOTONICS9080594.
44. G. T. Canbaz, Ü. Açikel, and Y. S. Açikel, "Green Synthesis of ZnO Nanoparticles from Onion Peel Wastes," pp. 1–5, 2020.
45. M. Y. Al-darwesh, S. S. Ibrahim, and M. A. Mohammed, "A review on plant extract mediated green synthesis of zinc oxide nanoparticles and their biomedical applications," Results in Chemistry, vol. 7, p. 101368, Jan. 2024, doi: 10.1016/J.RECHEM.2024.101368.
46. V. N. Jafarova and G. S. Orudzhev, "Structural and electronic properties of ZnO: A first-principles density-functional theory study within LDA(GGA) and LDA(GGA)+U methods," Solid State Communications, vol. 325, p. 114166, Feb. 2021, doi: 10.1016/J.SSC.2020.114166.
47. S. Abou Zeid and Y. Leprince-Wang, "Advancements in ZnO-Based Photocatalysts for Water Treatment: A Comprehensive Review," Crystals 2024, Vol. 14, Page 611, vol. 14, no. 7, p. 611, Jun. 2024, doi: 10.3390/CRYST14070611.
48. A. Sirelkhatim, S. Mahmud, A. Seeni, N. H. M. Kaus, L. C. Ann, S. K. M. Bakhori, H. Hasan, and D. Mohamad, "Review on Zinc Oxide Nanoparticles: Antibacterial Activity and Toxicity Mechanism," Nano-Micro Letters, vol. 7, no. 3, p. 219, Apr. 2015, doi: 10.1007/S40820-015-0040-X.
49. A. Nawaz, A. Farhan, F. Maqbool, H. Ahmad, W. Qayyum, E. Ghazy, A. Rahdar, A. M. Díez-Pascual, and S. Fathi-karkan, "Zinc oxide nanoparticles: Pathways to micropollutant adsorption, dye removal, and antibacterial actions - A study of mechanisms, challenges, and future prospects," Journal of Molecular Structure, vol. 1312, p. 138545, Sep. 2024, doi: 10.1016/J.MOLSTRUC.2024.138545.
50. K. Vallarasu, S. Dinesh, M. Nantha kumar, D. Mithun, R. Anitha, and V. Vijayalakshmi, "ZnO heterojunction photocatalysts prepared via facile green synthesis process attaining improved photocatalytic function for degradation of methylene blue dye," Desalination and Water Treatment, vol. 318, p. 100391, Apr. 2024, doi: 10.1016/J.DWT.2024.100391.
51. M. S, H. N, and V. P.P, "In Vitro Biocompatibility and Antimicrobial activities of Zinc Oxide Nanoparticles (ZnO NPs) Prepared by Chemical and Green Synthetic Route— A Comparative Study," BioNanoScience, vol. 10, no. 1, pp. 112–121, 2020, doi: 10.1007/s12668-019-00698-w.
52. N. K. Sharma, J. Vishwakarma, S. Rai, T. S. Alomar, N. AlMasoud, and A. Bhattarai, "Green Route Synthesis and Characterization Techniques of Silver Nanoparticles and Their Biological Adeptness," ACS Omega, vol. 7, no. 31, pp. 27004–27020, 2022, doi: 10.1021/acsomega.2c01400.
53. H. Hameed, A. Waheed, M. S. Sharif, M. Saleem, A. Afreen, M. Tariq, A. Kamal, W. A. Al-Onazi, D. A. Al Farraj, S. Ahmad, and R. M. Mahmoud, "Green Synthesis of Zinc Oxide (ZnO) Nanoparticles from Green Algae and Their Assessment in Various Biological Applications.," Micromachines, vol. 14, no. 5, Apr. 2023, doi: 10.3390/mi14050928.
54. A. Sirelkhatim, S. Mahmud, A. Seeni, N. H. M. Kaus, L. C. Ann, S. K. M. Bakhori, H. Hasan, and D. Mohamad, "Review on Zinc Oxide Nanoparticles: Antibacterial Activity and Toxicity Mechanism.," Nano-micro letters, vol. 7, no. 3, pp. 219–242, 2015, doi: 10.1007/s40820-015-0040-x.
55. A. R. Mendes, C. M. Granadeiro, A. Leite, E. Pereira, P. Teixeira, and F. Poças, "Optimizing Antimicrobial Efficacy: Investigating the Impact of Zinc Oxide Nanoparticle Shape and Size," Nanomaterials, vol. 14, no. 7, 2024, doi: 10.3390/nano14070638.